Diffusivity and hydrodynamic drag of nanoparticles at a vapor-liquid interface

Joel Koplik* and Charles Maldarelli†
Benjamin Levich Institute, Department of Chemical Engineering, and Department of Physics, City College of the City University of New York, New York, New York 10031, USA
(Received 7 July 2016; published 23 February 2017)

Measurements of the surface diffusivity of colloidal spheres translating along a vapor-liquid interface show an unexpected decrease in diffusivity, or increase in surface drag (from the Stokes-Einstein relation), when the particles situate further into the vapor phase. However, direct measurements of the surface drag from the colloid velocity due to an external force find the expected decrease with deeper immersion into the vapor. We perform molecular dynamics simulations of the diffusivity and force experiments for a nanoparticle with a small surface roughness at a vapor-liquid interface to examine the effect of contact line fluctuations. The drag calculated from both calculations agree and decrease as the particle positions further into the vapor. The surface drag is smaller than the bulk liquid drag due to the partial submersion into the liquid and the finite thickness of the interfacial zone relative to the nanoparticle size. We observe weak contact line fluctuations and transient pinning events, but these do not give rise to an anomalous increase in drag in this system.

DOI: 10.1103/PhysRevFluids.2.024303

I. INTRODUCTION

When a partially wetting colloidal particle breaches the interfacial zone between two adjoining immiscible fluid phases, the interfacial energy of the system is lowered, because the area of the fluid interface decreases and the contact areas of the particle with the bounding fluid phases are altered. Eventually the colloid comes to an equilibrium, representing a minimum in the interfacial free energy. For example, for a spherical colloid of radius R at a vapor-liquid interface of interfacial tension γ [Fig. 1(a)], the minimum free energy relative to the vapor phase is $\Delta\mathcal{F} = -\pi\gamma R^2(1+\cos\theta)^2$, where the contact angle θ is measured through the liquid and the immersion depth d is equal to $d/R = \cos\theta$ [1]. For particles of large enough size, $\Delta\mathcal{F}$ can overwhelm the typical thermal energy k_BT and the particle becomes trapped, as thermal fluctuations cannot dislodge the particle from the interface. Monolayers of strongly adsorbed colloids at the fluid interfaces of foams and emulsions provide steric barriers to coalescence of the dispersed phase and find applications as foam and (Pickering) emulsion stabilizers [1,2]. Particle stabilized foams and emulsions are also the starting points for material fabrication, including microcapsules with surfaces of fused colloids (colloidosomes) [3] and colloid-based foams, gels, and bijels [4]. Adsorbed colloidal monolayers on the surfaces of thin fluid films form, upon film evaporation, well-packed crystalline monolayers (see, e.g., Refs. [5–7] for a review) and these are useful as superhydrophobic or antireflection coatings, as templates for micro- and nanostructured materials (e.g., nanosphere lithography [8]), and as photonic crystals for optoelectronic devices (see the review by Prevo *et al.* [9]). Active colloids trapped at interfaces also serve as tracers for the measurement of the surface rheology (see, e.g., Refs. [10,11] and the review by Ortega *et al.* [12]).

An understanding of how colloids that are energetically trapped at a fluid interface organize and assemble is critical to the above applications as the microstructure determines the integrity and durability of the particle monolayers armoring bubbles and drops. The monolayer resilience

*jkoplik@ccny.cuny.edu
†cmaldarelli@ccny.cuny.edu

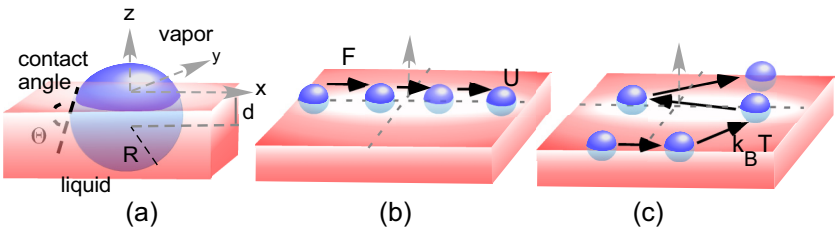

FIG. 1. (a) Spherical colloid of radius R and at immersion depth d at equilibrium at a vapor-liquid interface, (b) translation of a colloid along a surface at velocity U due to the action of an external force F applied parallel to the surface, and (c) surface diffusion of a colloid due to thermal fluctuation (Brownian) forces without external forcing.

accounts for the steric stabilization of foams and emulsions, and the strength of the microcapsule interfaces formed from the coated fluid particles. The colloid arrangement also directly determines the properties of the coatings and crystals formed from colloidal monolayers on thin films. Colloid assembly at interfaces is driven by the interaction forces between the particles [e.g., attractive forces due to capillarity and van der Waals interactions, and repulsive forces due to dipolar electrostatic or magnetic repulsion of charged (or magnetic) colloids], as well as external forces (electrical or magnetic fields) (for reviews see Refs. [13–19]). The colloid microstructure evolves as a balance between these interactions and the hydrodynamic viscous resistance due to the motion of the colloids along the surface. While the assemblage forces are well understood, knowledge of the hydrodynamic motion is incomplete, with, as we explain below, experiments providing anomalous results in light of the existing continuum and molecular dynamic theories for hydrodynamic drag. Hence here we study the hydrodynamics and in particular focus on the drag exerted on the floating colloids as they move along the interface.

Continuum calculations of the surface drag exerted on a spherical, smooth, nonrotating particle moving with velocity U due to an applied force F in rectilinear motion in the limit of zero inertia and at a flat zero-thickness interface separating two immiscible liquids have been undertaken using analytical and numerical methods [20–24] [Fig. 1(b)]. The translational drag coefficient ξ is the ratio of the applied force to the resulting velocity. The calculations demonstrate, as expected, that the continuum drag increases with immersion into the more viscous phase and approaches the Stokes bulk drag coefficient $6\pi\eta R$, where η is the fluid viscosity far from the surface. The shear flow due to the motion of the colloid creates a torque that acts to rotate the particle around the axis perpendicular to the motion and tangent to the surface. If the particle is smooth and chemically homogeneous, the particle rotates due to this applied torque with the contact line advancing over the surface of the leading side of the particle and receding over the trailing side, each with the same contact angle and the interface around the particle remaining flat. The torque is then balanced by rotational drag and the translational drag coefficient is less than the nonrotating colloid. However, the surfaces of most colloid particles are not homogeneous, but are characterized by either physical heterogeneities (surface roughness) or chemical heterogeneities. These heterogeneities can cause the contact line to intermittently become pinned as it moves (the line "hops" over inhomogeneities) and the line therefore advances or recedes with different effective angles (contact line hysteresis) dependent on the topology. Surface heterogeneities cause particles placed on the interface to show a slow equilibration as they settle to an equilibrium position because the interface becomes pinned at the heterogeneities [25–27]. In the context of a surface heterogeneous particle rotating due to the torque imposed by the shear flow due to the translation, the advancing and receding angles on the leading and trailing sides of the particle are not equal. This hysteresis causes the inclination angle of the fluid interface with the contact line to be asymmetric and creates an interfacial tension force that increases the fluid drag. In the limit in which the contact line becomes completely pinned and immobile, these tension forces can completely arrest the rotation [28].

The surface drag can also be obtained from the fluctuation in position of the colloid along the surface due only to Brownian thermal forces [Fig. 1(c)]. In this case the drag is related to the diffusivity D obtained from the ensemble-average mean-square displacement by the Stokes-Einstein relation $\xi = k_B T/D$. Molecular dynamics (MD) simulations have used this method to calculate the drag on smaller, nanometer-sized spherical rigid or structureless colloidal particles at an atomistically fluctuating liquid interface. Cheung [29] studied an interface separating monotonic Lennard-Jones fluids that are identical (i.e., the atom-atom interactions in each fluid are the same) and are made immiscible by a reduced interaction between the atoms of the two fluids. The calculated diffusion coefficient of spherical nanoparticles at the interface was less than the simulated bulk diffusion coefficient D. This is as expected, as the nanoparticle, which was symmetrically located at the interface, straddles an interface of finite width, and the reduced density and viscosity of the zone reduces the hydrodynamic drag, allowing greater dispersion. Similar MD simulations of a spherical colloid symmetrically placed at the interface of identical Lennard-Jones fluids by Rezvantalab *et al.* [30,31] demonstrated the reduced surface drag coefficient relative to the bulk; these authors also investigated the diffusion of Janus particles made of hemispheres that interacted selectively with the bounding fluids. Further Lennard-Jones MD simulations of the diffusivity at different particle immersion depths on a vapor-liquid interface showed the expected decrease in D with immersion into the liquid [32], as well as an MD simulation [33] of a water-polydimethylsiloxane interface with different bounding phase viscosities and realistic potentials, in which D was calculated to be between the simulated bulk diffusion coefficients. Interestingly, direct simulations of the surface drag coefficient through the measurement of the particle velocity due to a constant force were not undertaken and therefore a comparison of the drag coefficient from both methods (and validation of the Stokes-Einstein equation) was not undertaken.

Experiments have directly obtained the surface drag on large spherical colloids (1–10^3 μm in diameter) at gas-aqueous and oil-aqueous interfaces by moving the particles with magnetic [34] or capillary forces (see, e.g., [35,36]) and measuring the resultant velocity using optical microscopy and particle tracking. To compare with theory, the particle immersion depth is evaluated separately by a measurement of the contact angle, through either direct observation or, for smaller particles, interferometric measurements or gelling of the liquid (for gas-liquid interfaces) to make casts of the interface. The measured surface drag coefficient was found to be in agreement with the continuum predictions for the drag coefficient of a nonrotating particle and a flat interface.

However, in experiments on smaller spherical colloids (100 nm to 1 μm in diameter) in which the diffusivity is measured directly by particle tracking of the fluctuating position of the particle due to Brownian motion and the drag coefficient is computed from the Stokes Einstein relation, η is not always in agreement with continuum predictions and can show strikingly anomalous behavior in its dependence on the immersion depth of the colloid. At the decalin- (oil-) water interface, Peng *et al.* [37] measured for very hydrophobic particles a value for the diffusion equal to the value in the bulk oil phase and rationalized this result due to the presumed nearly complete immersion of the colloid in the oil. At the silicone oil–water interface, Du *et al.* [38], for partially wetting particles, obtained D intermediate between the bulk phase diffusivities, as would be expected. Similarly, for partially wetting particles at the air-water interface, Gehring and Fischer [39] obtained diffusion coefficients larger than values in the bulk because of the partial immersion of the colloid at the surface in the water. However, for a large number of experiments for partially wetting particles at the air-water interface, results have been obtained in which the surface diffusivity (for small contact angles) is larger than in the bulk but smaller than would have been predicted from continuum theory (cf. Refs. [40–42]) or (for large contact angles) the surface diffusivity is anomalously smaller than the bulk value (cf. Refs. [42–47]). For even smaller particles, O(10 nm) luminescent quantum dots or fluorescent dendrimers or dye molecules, for which the surface diffusivity was obtained at the linear alkane-water interface from fluorescence recovery after photobleaching or fluorescence correlation spectroscopy, the surface diffusivity was found to be smaller than the bulk diffusivity in oil when the oils were equal to or more viscous than the water phase [48], although dendrimers obeyed the continuum predictions [49].

Several mechanisms have been proposed to explain the unexpectedly low surface diffusivities. Obviously, surfactant contaminants could give rise to viscous surface shear and Marangoni forces, which increase the surface drag. However, tension measurements in some diffusion experiments indicate a relatively clean interface and attention has focused on the contact line at the particle surface, the thermal fluctuations in the line, and the inclination angle of the interface attached to the line [42]. As noted above, the surface of colloids is typically heterogeneous. As the colloid diffuses along the surface due to the thermal fluctuations, there are two possibilities for a heterogeneous particle. In the first, it rotates due the torque exerted by the translation and torque generated by thermal fluctuations. As it is forced to rotate, the contact line thermally hops between pinning sites at the forward and back ends of the particle, creating fluctuating differences in the advancing and receding angles, which gives rise to an additional drag force. Alternatively, the contact line can become permanently pinned at the heterogeneities and the colloid does not rotate at all. While the contact line stays in place during the fluctuations, the inclination angle of the interface attached to the colloid can still fluctuate due to capillary waves creating an additional drag. Thus, in either case, an additional drag develops due to the surface heterogeneity that augments the viscous drag.

The focus of this study is to understand the drag exerted on colloids with heterogeneous surfaces as they diffuse along an interface and specifically examine the role of contact line pinning and depinning, and fluctuations in the fluid inclination angle on the drag. We use molecular dynamics calculations to undertake the study, as these simulations can straightforwardly incorporate these effects on a heterogeneous surface. We adopt a model in which a nanoparticle is situated at a vapor-liquid interface of a Lennard-Jones fluid, with the nanoparticle composed of atoms cut from a spherical section of a lattice so that the particle surface is rough. Our objective is to use these MD simulations to determine whether fluctuations in the contact line or the interface slope at the contact line can account for the anomalously large surface drag measured in diffusion experiments. We will also compare the drag coefficients obtained from the diffusion experiments (through the Stokes-Einstein equation) to the coefficient obtained by direct calculation of the motion of the same particle subject to a constant force and compare these with the drag coefficient calculated from continuum studies. This comparison will help us understand the paradoxical result that the experimental drag coefficient obtained from forced motion of the colloid is in agreement with the continuum predictions.

II. METHODOLOGY FOR THE MOLECULAR DYNAMICS SIMULATION

The simulations employ basic MD methods [50,51]. We consider a slab of a bath of tetramer molecules in vapor-liquid equilibrium (vapor above liquid) composed of finitely extensible nonlinear elastic (FENE) chains of Lennard-Jones (LJ) atoms confined from below by a lattice of (LJ) atoms and from above by a hard potential [Fig. 2(a)]. The nanoparticle at the interface is composed of a lattice of LJ atoms. We denote by species 1 the atoms of the tetramer, by 2 the atoms of the nanoparticle, and by 3 the atoms of the base. The Lennard-Jones intermolecular interaction among the molecules is

$$V_{\mathrm{LJ}}(r) = 4\epsilon[(r/\sigma)^{-12} - c_{ij}(r/\sigma)^{-6}], \tag{1}$$

where σ is the core diameter (the same for all atoms), ϵ is the common energy scale, r is the separation distance between atoms, and the coefficients c_{ij} adjust the strength of the attractive interaction between atoms of atomic species i and j. All atoms have the same mass m and the LJ parameters define a time scale $\tau = \sigma(m/\epsilon)^{1/2}$. For the tetramer liquid (species 1) we adopt the standard value $c_{11} = 1.0$. The LJ potentials act between each pair of atoms within a cutoff range 2.5σ. The tethering FENE potential between the atoms of each tetramer is

$$V_{\mathrm{FENE}}(r) = -\frac{1}{2}k_F r_0^2 \ln\left(1 - \frac{r^2}{r_0^2}\right) \tag{2}$$

with its parameters given by $k_F = 30\epsilon/\sigma^2$ and $r_0 = 1.5\sigma$, following Ref. [52].

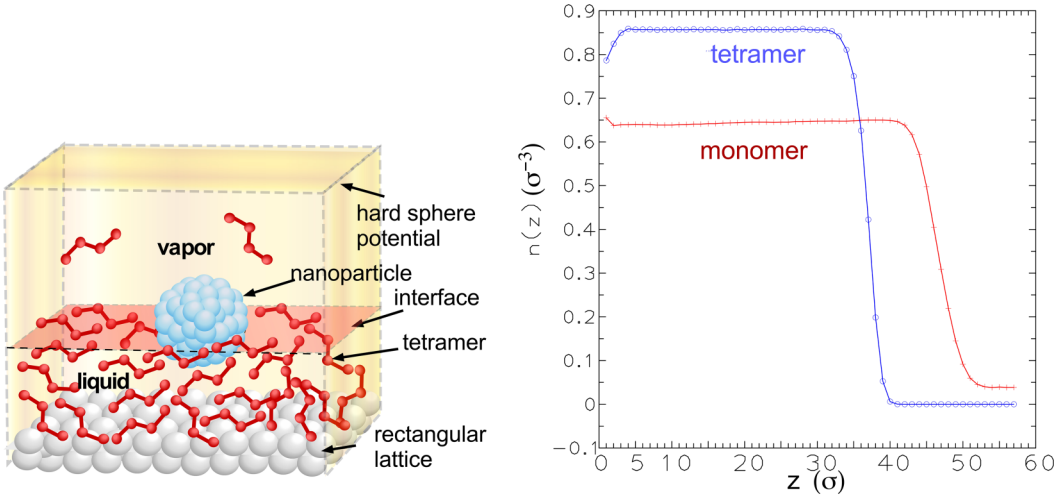

(a) (b)

FIG. 2. (a) Simulation cell consisting of a slab of tetramer molecules in vapor-liquid equilibrium confined from above by a hard potential and from below by a rectangular lattice of atoms with the nanoparticle at the interface and (b) density profile $n(z)$ across the interface for monomeric and tetrameric liquids.

The bottom lattice of species 3 atoms consists of two layers attached by linear tether springs to fcc lattice sites with interaction strength $c_{13} = c_{23} = c_{33} = 1.0$ as well. The latter value leads to a no-slip boundary condition so that the bottom wall can prevent free translation of the system. Periodic boundary conditions are imposed in both lateral directions and the equations of motion are integrated using predictor-corrector methods. A local Nosé-Hoover thermostat fixes the temperature at $0.8\epsilon/k_B$, for which the tetramer liquid and vapor are in equilibrium with a vapor-liquid surface tension (obtained by numerical integration of the difference between normal and transverse stress across the interface) $\gamma = 0.668\epsilon/\sigma^2$. The bulk liquid density is $0.857\sigma^{-3}$ and the viscosity is $\eta = 5.18m/(\sigma\tau)$, obtained from a separate simulation of the same liquid placed between two solid walls in Couette flow.

The solid particle (species 2) is a rigid spherical section of a cubic lattice of the same LJ atoms at the same bulk density as the equilibrated liquid, formed by enclosing all atoms of the lattice within a radius 8σ of a central atom, which yields a distinctly rough surface. The solid LJ atoms interact with the LJ tetramer atoms via the LJ potential with the same energy ϵ but an attractive interaction strength c_{12}, which is varied to adjust the wettability (the contact angle) and thereby vary the immersion depth. The interaction with the bottom lattice is set to $c_{23} = 1.0$. The particle motion is obtained by computing the net force and torque exerted on it by fluid atoms and translating and rotating it according to the Newton and Euler equations. Quaternion variables [50] are used to specify the orientation. There are 110 608 atoms in the liquid, 3600 in the solid base, and 1736 in the particle and the simulation box is a cube of side 60.3σ. If the parameters in the potential are given values appropriate for argon, the particle radius is about 2.5 nm and the intrinsic time unit $\tau = 2.12$ ps. The motivation for using tetrameric molecules is to sharpen the interface, which would be as broad as the particle itself in the monatomic case: The interfacial density profiles in the absence of a particle are shown in Fig. 2(b), which also demonstrates the vapor-liquid equilibrium.

III. IMMERSION DEPTH OF THE NANOPARTICLE AT THE INTERFACE

We first compute the immersion depth d [Fig. 1(a)] from simulations of diffusion. The particle is initially placed below the interface and allowed to migrate upward to its equilibrium position and diffuse there. The particles are not explicitly constrained to lie at the interface, and move in three

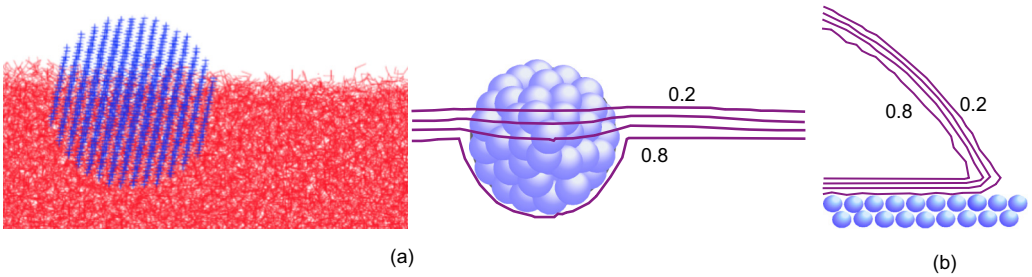

FIG. 3. (a) Snapshot of the simulated vapor-tetramer interface with the colloid particle and corresponding contour plot for $c_{12} = 0.9$ and (b) simulation of the cylindrical sessile drop of the tetramer on a solid substrate at $c_{12} = 0.9$. The lines are density contours spaced by 0.2, in units of σ^{-3}.

dimensions and do exhibit some vertical motion, but the typical height fluctuation is small with a standard deviation in the height distribution of at most 0.6σ, even for the lowest wettability. The immersion depth is based on the average horizontal position of the center of the particle relative to planes of isocontours of the fluid density far from the interface: See Fig. 3(a) for $c_{12} = 0.9$. The contours show that the particle radius R is comparable to the size of the interfacial transition zone. When the particle radius is much larger than the zone thickness, contours of different density do intersect the particle at the same angle, defining a unique contact angle and immersion depth. Here the contours intersect at different angles and the contact angle is ambiguous. We choose to define the immersion depth as the vertical distance from the half-bulk-density contour to the particle center, defining an apparent contact angle ($d/R = \cos\theta_A$). The apparent angle is plotted in Fig. 4(a) as a function of c_{12}. Note that the immersion into the liquid increases with the strength of the liquid-solid interaction c_{12}, in agreement with MD calculations of Cheng and Grest [32].

The apparent contact angle θ_A can be compared to the angle measured directly in analogous MD simulations of sessile drops of the tetramer on a planar substrate of atoms identical to the colloid and in the same lattice configuration [Fig. 3(b) for $c_{12} = 0.9$]. The large substrate area allows the

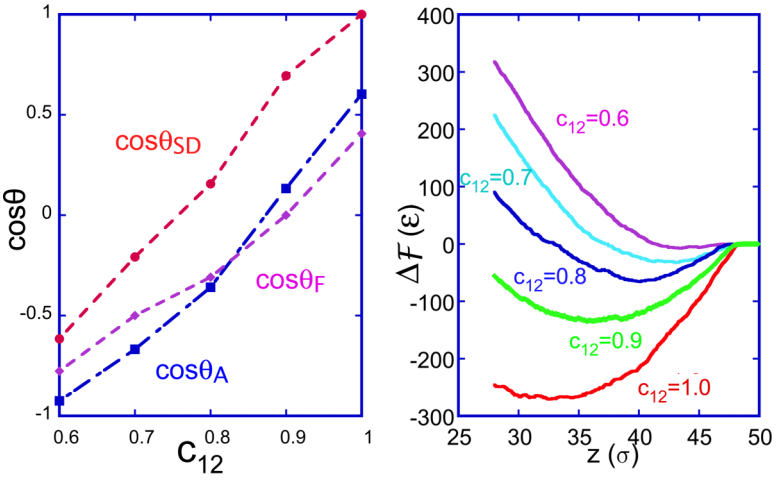

FIG. 4. (a) Contact angle θ as a function of c_{12} obtained from simulation (apparent angle θ_A), from a cylindrical sessile drop simulation θ_{SD}, and from free-energy calculation θ_F and (b) free energy $\Delta\mathcal{F}$ as a function of position z normal to the interface.

fluid interface contours to intersect it as a set of concentric circles, at nearly identical angles θ_{SD}, plotted alongside the apparent angles in Fig. 4(a). Note that $\theta_{SD} < \theta_A$ and can only be brought into congruence by defining d relative to a contour of lower density.

A second measure of the equilibrium immersion depth can be obtained by calculating the free energy of the system as a function of the vertical position of the particle by thermodynamic integration [53]. Since temperature is held fixed, the change in Helmholtz free energy between two immersion depths equals the work done when the particle is moved quasistatically and reversibly between the two points. Explicitly, $\Delta\mathcal{F} = \int \mathbf{F}(\mathbf{r}) \cdot d\mathbf{r}$, where $\mathbf{F}$ is the force on the particle at $\mathbf{r}$. To evaluate the integral, the liquid slab is equilibrated until the density field stabilizes. The particle is first placed in the nearly empty region above the interface and slowly displaced downward into the liquid, alternately moving it by 0.1σ at a velocity $0.001\sigma/\tau$, reequilibrating the system for 50τ and then averaging the force while it is fixed in position for 100τ. The results are given in Fig. 4(b) for the various wettabilities. In each case, including the completely wetting value $c_{12} = 1$, $\Delta\mathcal{F}$ is zero until the particle contacts the fluid, then dips, reflecting the attraction of the liquid atoms, and then displays a minimum inside the fluid at a position that deepens as the wettability increases. The curves flatten out at lower values of z fully inside the bulk liquid. The minimum is quite shallow for the case $c_{12} = 0.6$ where the particle is barely in contact with the fluid, indicating weak binding. A contact angle and immersion depth based on the free-energy minimum $\Delta\mathcal{F}/\pi R^2\gamma = -(1 + \cos\theta_F)^2$ is also plotted in Fig. 4(a).

IV. CALCULATION OF THE NANOPARTICLE DRAG COEFFICIENT

A. Drag coefficients of nanoparticles in the bulk

We begin our calculation of the surface drag coefficient by validating our simulations for a completely immersed colloid with no-slip boundary conditions ($c_{12} = 1$) in a constant force simulation. The colloid is placed in the center of a slab of liquid confined between two walls identical to the bottom wall of our vapor-liquid simulation cell and with the spacing adjusted to give the same bulk liquid density as when a liquid-vapor interface is present. We translate the colloid at a constant velocity through the middle of the channel and measuring the net force the fluid exerts on it. More precisely, at each time step Δt the center of mass of the particle is translated by $\boldsymbol{U}\Delta t$ while the particle is allowed to rotate according to the Euler equations in response to the net torque exerted on it by fluid atoms. The net force $\boldsymbol{F}_{\text{ext}}$ exerted by the fluid on the particle is recorded (but not used to update the center of mass position) and averaged over the duration of the simulation. Although the force fluctuates strongly from time step to time step, its average is quite stable when averaged over a time interval of 100τ or more. We define the drag coefficient ξ via $\boldsymbol{F}_{\text{ext}} = \xi\boldsymbol{U}$ and a bulk run of 1500τ yields $\xi_b = (756 \pm 30)m/\tau$. The result is in good agreement with the expected drag coefficient for a perfect no-slip sphere in low-Reynolds-number flow in an unbounded fluid $\xi_b = 6\pi\eta R = 781m/\tau$. Wall effects are negligible for a sphere of radius 8σ at the center of a channel of width 60σ: The correction to ξ_b is only about 0.2% [54] and comparable to the statistical error. The discrepancy may be attributed to the particle's surface roughness, which introduces some uncertainty in the definition of radius; we could define a hydrodynamic radius equal to 7.74σ. Likewise, the periodicity in the other two directions would modify the result, but we expect this effect to be similarly small.

We next compute ξ from simulations of the diffusivity of a completely immersed colloid using the same simulation cell of a liquid between two walls. In this case, the colloid is allowed to migrate to the interface and move freely according to Newton's law, based on the instantaneous force exerted by the fluid with no external forcing. We consider a statistical ensemble of 90 independent realizations, with different random seeds used to generate the initial velocity distribution, and record the average mean-square displacement as a function of time for simulations of $1.5 \times 10^4\tau$. In order to have a close comparison with the cases of particles at an interface where only diffusion in the plane of the interface is relevant and to minimize the effect of the confining walls, we focus on the two-dimensional diffusivity D in the plane parallel to the channel walls, which is related to the

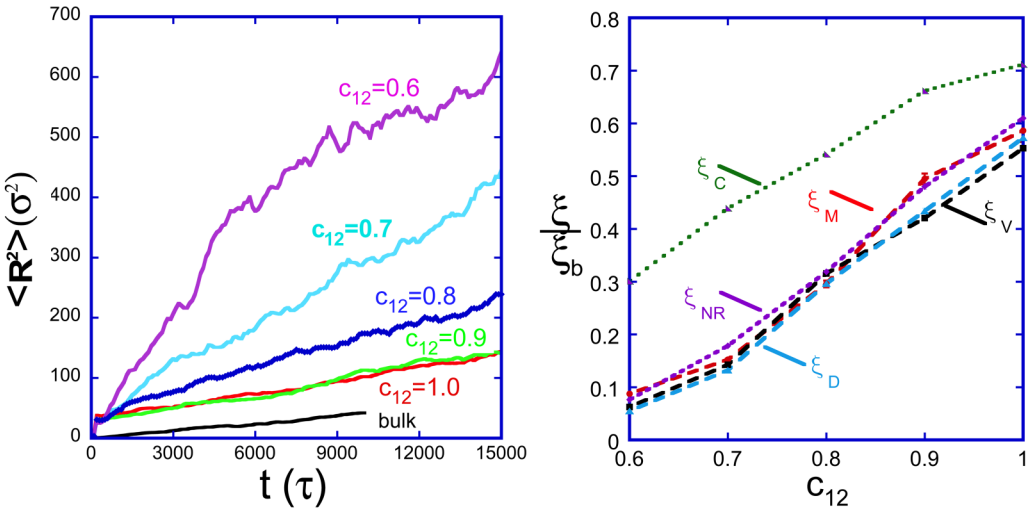

FIG. 5. (a) Mean-square displacement in the plane of the interface vs time for various wettabilities and (b) surface drag as a function of interaction parameter c_{12}. In (b), the various drag coefficients are ξ_C, continuum results for a no-slip sphere and a zero-thickness interface [24]; ξ_M, drag inferred from mean-square displacement measurements of diffusion, using the Stokes-Einstein relation; ξ_V, drag inferred from VACF measurements of diffusing spheres; ξ_D, directly measured drag on a freely rotating sphere pulled along the interface; and ξ_{NR}, directly measured drag on a nonrotating pulled sphere.

mean-square displacement by $\langle \mathbf{R}^2 \rangle \equiv \langle x^2 + y^2 \rangle = 4Dt$. The result, the black lower curve in Fig. 5(a), is a noisy straight line whose slope is determined by a least-squares fit to be $D_b = 0.0012\sigma^2/\tau$, which when inserted into the Stokes-Einstein relation $\xi = k_B T/D$ predicts a drag coefficient $\xi_b = (788 \pm 9)m/\tau$, again in good agreement with the constant external force drag calculation and the continuum prediction. We also record the instantaneous particle velocity as a function of time and compute the in-plane velocity autocorrelation function (VACF) $c(t) = \frac{1}{2}\langle\langle v_x(t+\tau)\, v_x(\tau) + v_y(t+\tau)\, v_y(\tau)\rangle\rangle$, where the angular brackets refer to an average over realizations and over the starting time τ. Mathematically, $D = \lim_{t\to\infty} \frac{1}{4t}\langle \mathbf{R}^2(t)\rangle = \lim_{t\to\infty} \int_0^t dt' c(t')$, but the two expressions treat the data differently and need not quite agree for finite samples and finite measurement times. In practice, the integral of the VACF first increases as a function of the upper limit, then reaches a plateau whose value is taken to be D, and then oscillates at larger values of t where the VACF fluctuates about zero. The resulting estimate, $D_b = 0.0011\sigma^2/\tau$ and $\xi_b = 792$, is quite consistent with the previous values. Finally, we note that the intercept of the VACF $c(0) = 4.60 \times 10^{-4}(\sigma/\tau)^2$ agrees with the value $k_B T/M$ (M the colloid mass) expected from the equipartition theorem and furthermore we observe that the probability distributions for the three particle velocity components are Gaussian with this width.

B. Surface drag coefficients for nanoparticles at the interface

We now calculate the surface drag coefficient ξ from diffusion [Fig. 1(c)] and constant force [Fig. 1(b)] simulations for colloids at an interface for different immersion depths. For the diffusion simulation, the two-dimensional mean-square displacement vs time is given in Fig. 5(a). As in the fully immersed case, the slope is determined by a least-squares fit and converted into a drag coefficient using the Stokes-Einstein relation; the results are recorded in Fig. 5(b) as ξ_M/ξ_b, as a function of c_{12}. We also measure the velocity autocorrelation in these simulations and its time integral provides a second, semi-independent determination of the diffusivity and is in good agreement with ξ_M [ξ_V in

TABLE I. Drag coefficient (in units m/τ) vs wettability, for different calculational methods: ξ_M, inferred from the mean-square displacement using the Stokes-Einstein relation; ξ_V, inferred from the VACF; ξ_D, direct measurement on a translating and rotating particle; ξ_{NR}, direct measurement on a nonrotating particle; and ξ_C, continuum Stokes equation calculation.

c	ξ_M	ξ_V	ξ_D	ξ_{NR}	ξ_C
0.6	69.0 ± 0.6	49.4	41.4 ± 0.8	57.7 ± 8.9	235
0.7	120 ± 1	113	100 ± 1.5	135 ± 2	343
0.8	233 ± 5	250	224 ± 3	241 ± 2	423
0.9	414 ± 8	333	328 ± 4	363 ± 4	517
1.0	462 ± 17	438	433 ± 6	461 ± 5	556

Fig. 5(b)]. For the calculation of ξ by the application of a constant force, for each wettability or value c_{12}, the particle is fixed at the mean height obtained in the diffusion calculation and dragged parallel to the interface at a fixed velocity $0.1\sigma/\tau$ while allowed to rotate freely; the ratio of force to velocity is recorded in Fig. 5(b) as ξ_D. (The unnormalized numerical values, along with their associated statistical errors, are given in Table I.) We see that the diffusion and constant force measures of ξ are within 10% agreement. The surface drag decreases as the particle displaces into the vapor phase and is always less than the drag in the bulk liquid. Importantly, the anomalously large drag that has been obtained when the particle situates further into the gas phase is not observed.

We also examined the limiting case in which the particle does not rotate in ϕ or θ by repeating the constant force simulation without allowing rotation. We find the drag ξ_{NR} to be expectedly larger than in the case of free rotation, but only marginally so [see Fig. 5(b)], and this restriction does not lead to an anomalously large drag. The Stokes continuum drag of a nonrotating smooth particle moving along a gas-liquid interface [20–22,24] is shown in Fig. 5(b) as ξ_c and is larger than the drag computed from the MD simulations. The interfacial width is the likely source of the discrepancy: The sphere in these simulations is partly in contact with lower density fluid in the interfacial zone, which exerts less force, as has also been found in Refs. [29,32].

C. Fluctuations in the contact line at the nanoparticle surface

To examine the contact line pinning and depinning during the simulations we have monitored the orientation of the particle with time when the colloid is simply diffusing or being dragged. To do this, we define a director [Fig. 6(a)] as the unit vector between two atoms at opposite sides of the

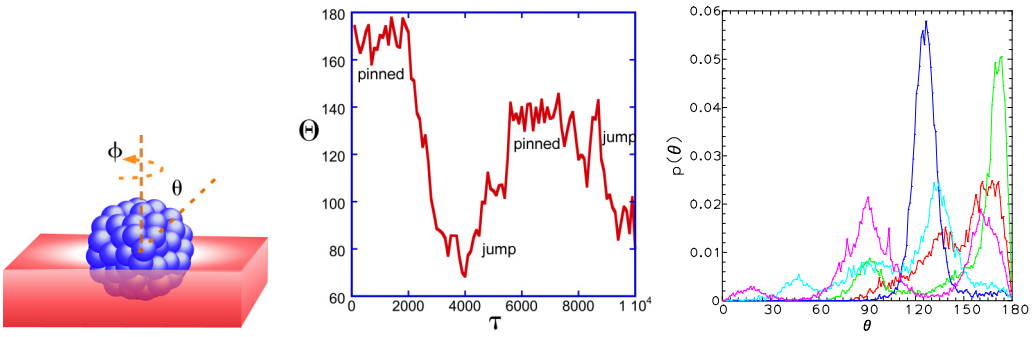

FIG. 6. (a) Definition of body angles θ and ϕ, (b) sample rotation angle θ during a diffusion simulation ($c_{12} = 0.7$), and (c) probability distributions for the orientation angle θ normal to the interface for different wettabilities. The color code is the same as in Figs. 2 and 3.

(rigid) particle and record its orientation angle as a function of time, both with respect to the interface normal (θ) and in the plane of the interface (ϕ). Visualizations of the interface such as Fig. 3(a) show a relatively planar surface intersecting the colloid so that the body fixed angle θ locates the contact line. To emphasize this point, we also provide a movie of a diffusion simulation with $c_{12} = 0.7$ for a nanoparticle diffusing freely for a 1000τ time interval (see [55]). The liquid-vapor interface shows some irregularity and displays obvious thermal fluctuations, but in all cases remains approximately flat, even at the surface of the particle. In individual diffusion runs, while ϕ tends to vary randomly, θ [see Fig. 6(b)] varies erratically, showing either intervals of continuous variation (no pinning or hopping) or intermittent jumps to orientations where it remains pinned. While expected for a rough surface, this contact line movement does not lead to large inclinations in the vapor-liquid interface [see Fig. 3(a) and [55]]. Evidently, the scale of the surface roughness on the nanoparticle is not large enough for jumping to create sufficient capillary forces to raise the drag as conjectured in Ref. [42] for large-scale heterogeneities on micron-sized particles and hence our results do not contradict the model proposed in Ref. [42].

An alternative way to examine the orientational behavior of the particles during the diffusion runs is to average over the different realizations to obtain the probability distribution functions for the two angles. Unfortunately, the results must be regarded as transient since the simulations do not run long enough to fully sample the angular distributions. The characteristic rotational diffusion time T_r is the inverse of the rotational diffusivity, and using the Stokes-Einstein relation again, $T_r = 1/D_r = \xi_r/k_BT = 8\pi\eta R^3/k_BT = 8.33 \times 10^4\tau$, which rather exceeds the duration of the simulations here. The transient probability distribution functions for θ over a 1000τ interval for different wettabilities are shown in Fig. 6(c). We see no, one, or two peaks, at different angles in different wettabilities, with no obvious pattern. The corresponding distribution for the in-plane angle ϕ is similarly devoid of a clear pattern and generally is a much noisier version of this figure.

V. CONCLUSION

To conclude, in all cases of nanoparticles with a rough surface at a vapor-liquid interface, the drag coefficient inferred from diffusion MD simulations and the Stokes-Einstein relation is in agreement with the drag coefficient ξ obtained from the constant force MD simulations, which show that the drag decreases as the colloid becomes more immersed in the gas phase. Since the size of the nanoparticle was comparable to the thickness of interfacial zone, the surface drags were less than values computed from continuum studies with a sharp interface. While contact line pinning and depinning is observed in the diffusion simulations, they do not create large surface drag as underscored by the fact that MD simulations for a pinned nonrotating colloid dragged across the surface has a surface drag only slightly larger than the free-rotating case.

ACKNOWLEDGMENT

J.K. was supported in part by NSF Grant No. CBET-1264550.

[1] B. Binks, Particles as surfactants—Similarities and differences, Curr. Opin. Colloid Interface Sci. **7**, 21 (2002).

[2] *Colloidal Particles at Liquid Interfaces*, edited by B. Binks and T. Horozov (Cambridge University Press, Cambridge, 2006).

[3] A. D. Dinsmore, M. F. Hsu, M. G. Nikolaides, M. Marquez, A. R. Bausch, and D. A. Weitz, Colloidosomes: Selectively permeable capsules composed of colloidal particles, Science **298**, 1006 (2002).

[4] M. E. Cates and P. S. Clegg, Bijels: A new class of soft materials, Soft Matter **4**, 2132 (2008).

[5] N. D. Denkov, O. Velev, P. A. Kralchevsky, I. B. Ivanov, H. Yoshimura, and K. Nagayama, Mechanism of formation of two dimensional crystals from latex particles on substrates, Langmuir **8**, 3183 (1992).
[6] N. D. Denkov, O. Velev, P. A. Kralchevsky, I. B. Ivanov, H. Yoshimura, and K. Nagayama, Two dimensional crystallization, Nature (London) **361**, 26 (1993).
[7] N. Vogel, M. Retsch, C.-A. Fustin, A. del Campo, and U. Jonas, Advances in colloidal assembly: The design of structure and hierarchy in two and three dimensions, Chem. Rev. **115**, 6265 (2015).
[8] F. Burmeister, C. Schafle, T. Matthes, M. Bahmisch, J. Boneberg, and P. Leiderer, Colloid monolayers as versatile lithographic masks, Langmuir **13**, 2983 (1997).
[9] B. Prevo, D. Kuncicky, and O. Velev, Engineered deposition of coatings from nano- and micro-particles: A brief review of convective assembly at high volume fraction, Colloids Surf. A **311**, 2 (2007).
[10] C. F. Brooks, G. G. Fuller, C. W. Frank, and C. R. Robertson, An interfacial stress rheometer to study rheological transitions in monolayers at the air-water interface, Langmuir **15**, 2450 (1999).
[11] S. Q. Choi, S. Steltenkamp, J. A. Zasadzinski, and T. M. Squires, Active microrheology and simultaneous visualization of sheared phospholipid monolayers, Nat. Commun. **2**, 312 (2011).
[12] F. Ortega, H. Ritacco, and R. G. Rubio, Interfacial microrheology: Particle tracking and related techniques, Curr. Opin. Colloid Interface Sci. **15**, 237 (2010).
[13] P. A. Kralchevsky and K. Nagayama, Capillary interactions between particles bound to interfaces, liquid films and biomembranes, Adv. Colloid Interface Sci. **85**, 145 (2000).
[14] P. A. Kralchevsky and K. Nagayama, *Particles at Fluid Interfaces and Membranes: Attachment of Colloid Particles and Proteins to Interfaces and Formation of Two Dimensional Arrays* (Elsevier, Amsterdam, 2001).
[15] P. A. Kralchevsky and N. D. Denkov, Capillary forces and structuring in layers of colloid particles, Curr. Opin. Colloid Interface Sci. **6**, 383 (2001).
[16] P. Singh, D. Joseph, and N. Aubry, Dispersion and attraction of particles floating on fluid-liquid surfaces, Soft Matter **6**, 4310 (2010).
[17] D. Vella, Floating versus sinking, Annu. Rev. Fluid Mech. **47**, 115 (2015).
[18] F. Bresme and M. Oettel, Nanoparticles at fluid interfaces, J. Phys.: Condens. Matter **19**, 413101 (2007).
[19] J. Bleibel, A. Dominiguez, and M. Oettel, Colloidal particles at fluid interfaces: Effective interactions, dynamics and gravitation-like instability, Eur. Phys. J. Spec. Top. **222**, 3071 (2013).
[20] K. D. Danov, R. Dimova, and B. Pouligny, Viscous drag of a solid sphere straddling a spherical or flat surface, Phys. Fluids **12**, 2711 (2000).
[21] C. Pozrikidis, Particle motion near and inside an interface, J. Fluid Mech. **575**, 333 (2007).
[22] T. M. Fischer, P. Dhar, and P. Heinig, The viscous drag of spheres and filaments moving in membranes or monolayers, J. Fluid Mech. **558**, 451 (2006).
[23] A. Dani, G. Keiser, M. Yeganeh, and C. Maldarelli, Hydrodynamics of particles at an oil–water interface, Langmuir **31**, 13290 (2015).
[24] A. Dorr, S. Hardt, H. Masoud, and H. Stone, Drag and diffusion coefficients of a spherical particle attached to a fluid-fluid interface, J. Fluid Mech. **790**, 607 (2016).
[25] D. M. Kaz, R. McGorty, M. Mani, M. P. Brenner, and V. N. Manoharan, Physical ageing of the contact line on colloidal particles at liquid interfaces, Nat. Mater. **11**, 138 (2012).
[26] C. E. Colosqui, J. F. Morris, and J. Koplik, Colloidal Adsorption at Fluid Interfaces: Regime Crossover from Fast Relaxation to Physical Aging, Phys. Rev. Lett. **111**, 028302 (2013).
[27] A. M. Rahmani, A. Wang, V. N. Manoharan, and C. E. Colosqui, Colloidal particle adsorption at liquid interfaces: Capillary driven dynamics and thermally activated kinetics, Soft Matter **12**, 6365 (2016).
[28] A. Dorr and S. Hardt, Driven particles at fluid interfaces acting as capillary dipoles, J. Fluid Mech. **770**, 5 (2015).
[29] D. Cheung, Molecular simulation of nanoparticle diffusion at fluid interfaces, Chem. Phys. Lett. **495**, 55 (2010).
[30] H. Rezvantalab, G. Drazer, and S. Shojaei-Zadeh, Molecular simulation of translational and rotational diffusion of Janus nanoparticles at liquid interfaces, J. Chem. Phys. **142**, 014701 (2015).
[31] H. Rezvantalab and S. Shojaei-Zadeh, Tilting and tumbling of Janus nanoparticles at sheared interfaces, ACS Nano **10**, 5354 (2016).

[32] S. Cheng and G. Grest, Structure and diffusion of nanoparticle monolayers floating at liquid/vapor interfaces: A molecular dynamics study, J. Chem. Phys. **136**, 214702 (2012).
[33] Y. Song, M. Luo, and L. Dai, Understanding nanoparticle diffusion and exploring interfacial rheology using molecular dynamics simulations, Langmuir **26**, 5 (2009).
[34] J. Ally and A. Amirfazli, Magnetophoretic measurement of the drag force on partially immersed microparticles at air-liquid interfaces, Colloids Surf. A **360**, 120 (2010).
[35] J. T. Petkov, N. D. Denkov, K. D. Danov, O. D. Velev, R. Aust, and F. Durst, Measurement of the drag coefficient of spherical particles attached to fluid interfaces, J. Colloid Interface Sci. **172**, 147 (1995).
[36] M.-J. Dalbe, D. Cosic, M. Berhanu, and A. Kudrolli, Aggregation of frictional particles due to capillary attraction, Phys. Rev. E **83**, 051403 (2011).
[37] Y. Peng, W. Chen, T. Fischer, D. Weitz, and P. Tong, Short-time self-diffusion of nearly hard spheres at an oil-water interface, J. Fluid Mech. **618**, 243 (2008).
[38] K. Du, J. Liddle, and A. Berglund, Three dimensional real time tracking of nanoparticles at an oil-water interface, Langmuir **28**, 9181 (2012).
[39] T. Gehring and T. M. Fischer, Diffusion of nanoparticles at an air/water interface is not invariant under a reversal of the particle charges, J. Phys. Chem. C **115**, 23677 (2011).
[40] M. Sickert, F. Rondelez, and H. Stone, Single-particle Brownian dynamics for characterizing the rheology of fluid Langmuir monolayers, Europhys. Lett. **79**, 66005 (2007).
[41] M. Sickert and F. Rondelez, Shear Viscosity of Langmuir Monolayers in the Low-Density Limit, Phys. Rev. Lett. **90**, 126104 (2003).
[42] G. Boniello, C. Blanc, D. Fedorenko, M. Medfai, N. Mbarek, M. In, M. Gross, A. Stocco, and M. Nobili, Brownian diffusion of a partially wetted colloid, Nat. Mater. **14**, 908 (2015).
[43] B. Radoev, M. Nedjalkov, and V. Djakovich, Brownian motion at liquid-gas interfaces. 1. diffusion coefficients of macroparticles at pure interfaces, Langmuir **8**, 2962 (1992).
[44] P. Dhar, V. Prasad, E. Weeks, T. Bohlein, and T. M. Fischer, Immersion of charged nanopartilces in a salt solution/air interface, Phys. Chem. B **112**, 9565 (2008).
[45] A. Maestro, L. J. Bonales, H. Ritacco, T. M. Fischer, R. G. Rubio, and F. Ortega, Surface rheology: Macro-and microrheology of poly(tert-butyl acrylate) monolayers, Soft Matter **7**, 7761 (2011).
[46] W. Chen and P. Tong, Short-time self-diffusion of weakly charged silica spheres at aqueous interfaces, Europhys. Lett. **84**, 28003 (2008).
[47] J. R. Samaniuk and J. Vermant, Micro and macrorheology at fluid-fluid interfaces, Soft Matter **10**, 7023 (2014).
[48] D. Wang, S. Yordanov, H. M. Paroor, A. Mukhopadhyay, C. Y. Li, H.-J. Butt, and K. Koynov, Probing diffusion of single nanoparticles at water-oil interfaces, Small **7**, 3502 (2011).
[49] D. Wang, L. Pevzner, C. Li, K. Peneva, C. Y. Li, D. Y. C. Chan, K. Mullen, M. Mezger, K. Koynov, and H.-J. Butt, Layer with reduced viscosity at water-oil interfaces probed by fluorescence correlation spectroscopy, Phys. Rev. E **87**, 012403 (2013).
[50] M. Allen and Tildesley, *Computer Simulation of Liquids* (Oxford University Press, Oxford, 1987).
[51] D. Frenkel and B. Smit, *Undertstanding Molecular Simulation*, 2nd ed. (Academic, New York, 2002).
[52] G. S. Grest and K. Kremer, Molecular dynamics simulation for polymers in the presence of a heat bath, Phys. Rev. A **33**, 3628 (1986).
[53] S. Razavi, J. Koplik, and I. Kretzschmar, The effect of capillary bridging on the Janus particle stability at the interface of two immiscible liquids, Soft Matter **9**, 4585 (2013).
[54] L. Pasol, M. Martin, M. L. Ekiel-Jezewska, E. Wajnryb, J. Blawzdziewicz, and F. Feuillebois, Motion of a sphere parallel to plane walls in a poiseuille flow. Application to field-flow fractionation and hydrodynamic chromatography, Chem. Eng. Sci. **66**, 4078 (2011).
[55] See Supplemental Material at http://link.aps.org/supplemental/10.1103/PhysRevFluids.2.024303 for a movie of a diffusion simulation with $c_{12} = 0.7$ for a nanoparticle diffusing freely for a 1000τ time interval.